Benchmarking London dispersion corrected density functional theory for noncovalent ion-π interactions[†]

Sebastian Spicher,[a] Eike Caldeweyher ,[a] Andreas Hansen,[a*] and Stefan Grimme[a*]

The strongly attractive noncovalent interactions of charged atoms or molecules with π-systems are important binding motifs in many chemical and biological systems. These so-called ion-π interactions play a major role in enzymes, molecular recognition, and for the structure of proteins. In this work, a molecular test set termed IONPI19 is compiled for inter- and intramolecular ion-π interactions, which is well balanced between anionic and cationic systems. The IONPI19 set includes interaction energies of significantly larger molecules (up to 133 atoms) than in other ion-π test sets and covers a broad range of binding motifs. Accurate (local) coupled cluster values are provided as reference. Overall, 19 density functional approximations, including seven (meta-)GGAs, eight hybrid functionals, and four double-hybrid functionals combined with three different London dispersion corrections, are benchmarked for interaction energies. DFT results are further compared to wave function based methods such as MP2 and dispersion corrected Hartree–Fock. Also, the performance of semiempirical QM methods such as the GFNn-xTB and PMx family of methods is tested. It is shown that dispersion-uncorrected DFT underestimates ion-π interactions significantly, even though electrostatic interactions dominate the overall binding. Accordingly, the new charge dependent D4 dispersion model is found to be consistently better than the standard D3 correction. Furthermore, the functional performance trend along Jacob's ladder is generally obeyed and the reduction of the self-interaction error leads to an improvement of (double) hybrid functionals over (meta-)GGAs, even though the effect of the SIE is smaller than expected. Overall, the double-hybrids PWPB95-D4/QZ and revDSD-PBEP86-D4/QZ turned out to be the most reliable among all assessed methods in predicting ion-π interactions, which opens up new perspectives for systems where coupled cluster calculations are no longer computationally feasible.

1 Introduction

Ion-π interactions refer to strongly attractive noncovalent interactions (NCI) between ions and mostly organic π-systems.[1,2] They are of crucial importance for many processes in chemistry and biology, such as controlling the regio- and stereoselectivity in organic reactions,[3,4] enabling important biological processes,[5–9] and determining the structures of molecules and proteins.[10–13] The application of quantum mechanical (QM) methods in the description of such ion-π systems is desirable for an in depth understanding. Kohn–Sham Density Functional Theory (DFT), with its vast number of density functional approximations (DFA), is one of the most promising electronic structure methods for this purpose regarding accuracy and computational efficiency.[14,15] Nevertheless, DFT methods have well-known weaknesses, like the one-

and many-electron self-interaction error (SIE),[16–18] errors due to nondynamical correlation effects,[19,20] and the lack of long-range electronic correlation, so-called London dispersion (LD) interactions.[21] The effect on ion-π interactions is shown in this work.

The SIE affects even modern DFAs and may lead to severe SCF convergence problems,[22] artificial charge-transfer (CT),[23,24] and inaccurate NCI energies for larger inter-fragment distances. This is in contrast to Hartree–Fock (HF) theory and second-order Møller-Plesset perturbation theory (MP2), which are SIE free because the exchange integrals exactly cancel the self-interaction contributions from the Coulomb integrals. This behavior is exploited by hybrid DFAs where a fraction of exact exchange (also called Fock exchange) is mixed in, partially canceling the SIE. While large amounts of Fock exchange reduce the SIE, the resulting hybrid DFAs also inherit general shortcomings of HF, *e.g.*, a lacking description of Coulomb interactions by overestimating ionic contributions in the wave function. For a more general discussion on the one-electron SIE in DFT see, *e.g.*, Ref. 25, and for the related many-electron SIE see, *e.g.*, Ref. 17.

Mean-field electronic structure methods like HF do not describe long-range electronic correlation effects and hence cannot account for LD interactions. This drawback of HF is also present

in DFT. The absence of LD interactions is long known[26] and various solutions have been developed in the context of LD-corrected DFT methods.[21,27–30] One strategy to fix the dispersion problem of conventional DFT has been the development of additive corrections. A popular and frequently used additive scheme is the "DFT-D3" correction, where the majority of the missing dispersion energy is accounted for by summing up the dispersion contributions of each atom pair.[21,31,32] Another approach is to add the nonlocal (NL) correlation energy effects as a function of the electron density to standard exchange-correlation DFAs, which is known as van der Waals density functional theory (vdW-DFT),[33] or approximations thereof (VV10).[34]

For the development and testing of state-of-the-art DFT methods, ion-π interactions as a class of NCIs are of special interest. Symmetry adapted perturbation theory[35–37] (SAPT) studies, which allow the separation into different energy components namely electrostatics, Pauli repulsion, induction, and LD, revealed that ion-π systems incorporate strong electrostatic and inductive components.[38] For highly polarizable systems, however, also LD were identified as a crucial part of the ion-π interaction.[39] For this reason, ion-π interactions present a challenge for the density functional itself as well as for the added dispersion correction. In this work we introduce a benchmark set composed of 19 molecules with strong ion-π interactions. It is termed IONPI19 and contains significantly larger molecules than in existing compilations and is well balanced between anionic and cationic systems. Various common "real-life" binding situations are covered as they occur in protein structures, molecular recognition, and supramolecular receptors. Intramolecular ion-π interactions are included as well. Hence, the IONPI19 set is an interesting test case for DFT and an important addition to the pool of available benchmark sets.

As has been shown in previous studies,[40,41] well performing LD-corrected DFAs are able to reproduce coupled cluster reference interaction energies for cation-anion complexes, representing the building blocks of ionic liquids. These chemically often rather saturated systems are less prone to the SIE. Good results for small charged systems could also be obtained with DFT-D methods in Refs. 37 and 42, even though the benchmark sets discussed in these studies are composed of rather small ion-π systems. In this work, we want to find out if previous trends and findings also hold true for the IONPI19 set and we want to investigate the general importance of LD corrections for prototypical systems composed of cations/anions and π-systems. The common believe is that ion-π systems are dominated by electrostatic and inductive interactions[39] but little attention has been paid so far to the importance of LD in this context. In the present work, we will put a particularly focus on the latter in the framework of LD-corrected DFT. Also MP2 (see *e.g.*, Refs. 43,44) and variants thereof[45] are common methods for modeling ion-π interactions, although there are severe and well-known problems such as the overestimation of NCIs involving π-systems, particularly for π-π interactions.[46–50] Furthermore, similar to other post-HF correlation methods, MP2 is highly susceptible to the basis set superposition error[51,52] (BSSE), which leads to systematic overbinding with small and medium sized atom-centered basis sets. Due to

persisting popularity of MP2 in NCI studies (see *e.g.*, Refs. 53,54), it is evaluated here as a competitor method.

To evaluate the performance of the methods mentioned above, reliable reference values of high accuracy are needed. For small to medium sized systems (up to about 30 atoms) explicitly correlated coupled cluster composite schemes such as the Weizmann protocols[55] (W1-F12 and W2-F12) have proven to yield highly accurate reference values. Yet, the respective computational cost are considerable. For larger systems (up to about 150 atoms), domain based local pair natural orbital coupled cluster theory (DLPNO-CCSD(T))[56,57] is still computational feasible and was already successfully applied,[58,59] even though the high accuracy of the Wn-F12 protocols cannot be fully achieved. To reduce the additional errors due to the local (DLPNO) approximations, very tight threshold settings have to be applied[60] in addition to a proper complete basis set (CBS) extrapolation, which in turn also makes these calculations quite computationally demanding. The high-level reference values calculated in this work can also be very useful in the development and validation of low-cost methods, *e.g.*, of special force-fields (FF),[61,62] since hardly any reliable coupled-cluster reference values for ion-π interactions energies of larger molecules exist so far[63] and neither have them been calculated with such an accurate setup.[64] The development of such FFs and respective workflows is an emerging field of research, especially with respect to the efficient description of ion-π interactions in proteins.[65,66]

First, a brief survey of the employed semi-classical LD-correction schemes is given followed by a description of the compiled IONPI19 benchmark set. Further, the results for this test set are presented and discussed for all employed methods. An energy decomposition analysis (EDA) is performed for the dissociation of an ion-π complex to investigate the effect of the SIE for GGA and hybrid DFAs. Due to significant increases in efficiency, accuracy, and related popularity, semiempiraical QM (SQM) and FF methods are additionally tested and evaluated on the IONPI19 set. Timings are compared for all different types of methods with regard to their accuracy. Finally, general conclusions and method recommendations will be given.

2 Semi-classical London dispersion corrections

To account for the missing LD interactions in the framework of DFT (and also HF), we apply two closely related semi-classical LD-correction schemes. First, the widely used DFT-D3 method with two-body contributions (only $E_{\text{disp}}^{(2)}$) with the standard Becke–Johnson (BJ) rational damping.[67,68] Second, we consider the default version of the recently introduced DFT-D4 scheme[69–71] including also three-body Axilrod–Teller–Muto[72,73] (ATM) contributions, where the dispersion energy is given by

$$E_{\text{disp}}^{\text{DFT-D4}} = E_{\text{disp}}^{(2)} + E_{\text{disp}}^{\text{ATM}}. \tag{1}$$

The basic formula for two-body dispersion interactions is the same in the D3 and D4 model, where the BJ rational damping form for the interatomic pair sum is employed,
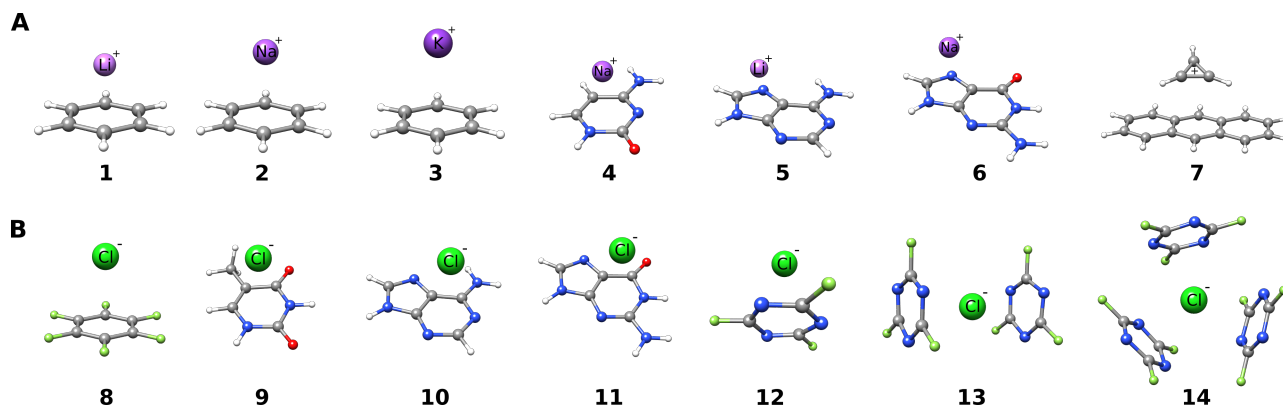
Fig. 1 Subset of the IONPI19 benchmark set containing small molecules ($\leq$ 30 atoms). **A** Systems **1-7** include cation-π interactions. **B** Systems **8-13** include anion-π interactions.

$$E_{\mathrm{disp}}^{(2)} = -\sum_{AB} \left[\frac{C_6^{AB}}{R_{AB}^6 + f\left(R_{AB}^0\right)^6} + s_8 \frac{C_8^{AB}}{R_{AB}^8 + f\left(R_{AB}^0\right)^8} \right], \quad (2)$$

with the three fitted damping and scaling parameters a_1, a_2, and s_8. Here, AB labels atom pairs, and $f(R_{AB}^0) = a_1 R_{AB}^0 + a_2$ is the BJ damping function with appropriate covalent radii.[32]

In both methods, the C_6 (and C_8) coefficients are obtained from precalculated frequency-dependent time-dependent DFT dipole polarizabilities.[74] In addition to the coordination number dependence in DFT-D3, classical atomic partial charges are included in DFT-D4, which are calculated by a charge model based on electronegativity equilibration of Gaussian type charge densities (EEQ).[75] According to many tests on neutral organic systems, DFT-D3 and DFT-D4 methods provide both accurate asymptotic dispersion energies of roughly coupled-cluster accuracy[21] while D4 is somewhat superior for ionic or metallic cases.[69,76] If this also holds for the important class of ion-π complexes is one of the main questions of the present work. Due to the high computational efficiency of the additive DFT-D schemes, they are also suitable for low-cost methods including force-fields.[77–81]

Other popular LD correction schemes exist, *e.g.*, the exchange-hole dipole method,[82–85] the many-body dispersion model,[27,86] the van der Waals family of density functionals,[87] or the non-local electron density dependent dispersion correction termed VV10 or DFT-NL.[34,88,89] For comparison, the latter is also tested in this work. For an in-depth analysis of other LD corrections and a more general discussion on the importance of LD effects for chemical bonding, see, *e.g.*, Refs. 21,30.

3 Description of the molecular test set

The composition of the test set aims at both, smaller model systems as well as experimentally investigated ion-π systems. We arrived (after considering more than 30 candidate structures) at a statistically balanced set containing 19 exemplary systems featuring typical ion-π binding motifs. The average system size is about 32 atoms per molecule with the largest system consisting of 133 atoms. The test set is divided in smaller ($\leq$ 30 atoms) and larger ($>$ 30 atoms) systems, of which the first subset is shown in Figure 1 and the latter in Figure 2. For the ten cationic and nine

anionic systems the mean interaction energy is -20.9 kcal mol^{-1}. Reference energies and estimated errors for each system as well as the corresponding computational reference level of theory are listed in Table 1.

Figure 1A shows the first seven systems of the IONPI19 set which are all cationic. Systems **1-3** show Li$^+$, Na$^+$, and K$^+$ bound to benzene. The three alkali-benzene complexes were taken from the CHB6 benchmark set[37,42] with the original reference interaction energies obtained at the CCSD(T)/CBS level of theory. Cation-π interactions are of particular interest for structural biology as the DNA bases are also able to participate therein. Systems **4-6** show Na$^+$ in complex with cytosine, Li$^+$ coordinated to the five-membered ring of adenine, and Na$^+$ in complex with the five-membered ring of guanine. The systems were taken from Ref. 90, where reference binding energies were also computed at the CCSD(T)/CBS level of theory. System **7** was newly added to this benchmark and consists of anthracene and the cyclopropenyl cation (C$_3$H$_3^+$). The reference interaction energy of the rigid monomers was computed at the W1-F12 level.

The anionic systems of the small molecule subset are shown in Figure 1B. For **8** the anion-π interaction of hexafluorobenzene (C$_6$F$_6$) and chloride (Cl$^-$) is achieved by placing strong electron withdrawing substituents along the π-system. The reference interaction energy was computed at the W1-F12 level. Systems **9-11** show chlorine anions in complex with the six-membered ring of thymine, adenine, and guanine. These systems and their respective reference interaction energies were taken from Ref. 90. The test systems **12-14** are newly added to this benchmark and were taken from a study on designing receptors for molecular recognition. There, the additivity of anion-π interactions for 1:1, 1:2, and 1:3 (anion:π) complexes of trifluoro-1,3,5-triazine (C$_3$F$_3$N$_3$) with Cl$^-$ ions[91] was investigated. All three systems were newly compiled for the IONPI19 set. Reference energies for the 1:1 complex were calculated at the W2-F12 level whereas the 1:2, and 1:3 complex were computed at the DLPNO-CCSD(T) / *VeryTightPNO* / CBS(aug-cc-pVTZ/aug-cc-pVQZ) level of theory.

The subset of larger molecules shown in Figure 2 was newly compiled for this work. **15** and **16** show the electron-deficit and cavity self-tunable macrocyclic host tetraoxacalix[2]arene-[2]triazine forming 1:1 complexes with small anions (NO$_3^-$,
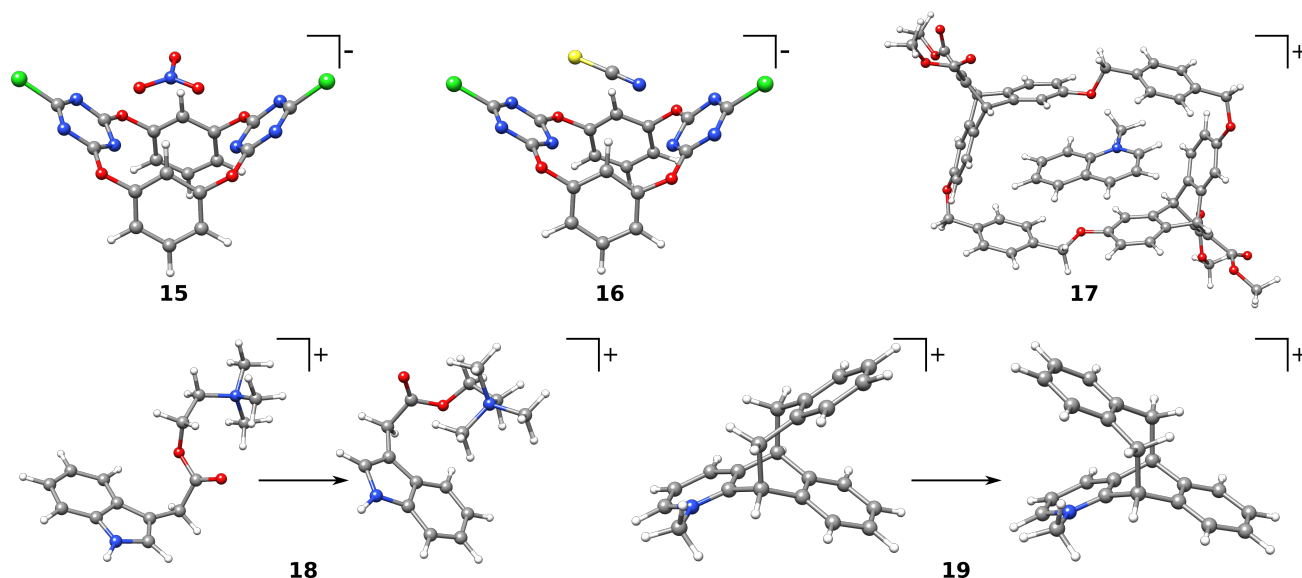
Fig. 2 Subset of the IONPI19 benchmark containing large molecules (> 30 atoms). System **15-17** show intermolecular ion-π interaction, whereas **18** and **19** are examples for intramolecular ion-π interactions.

SCN$^-$) as revealed by Wang and co-workers.[92] In complex, the two opposing triazine rings of tetraoxacalix[2]arene[2]triazine act as a pair of tweezers to interact with the included anions through cooperative anion-π and lone-pair electron-π interactions. The supramolecular cyclophane host-guest complex **17** is another interesting test system of practical relevance. This complex is able to catalyse N-alkylation to form cationic products *via* the Menschutkin reaction,[93] where it is assumed that the cation-π interaction plays a central role in catalysis. Hence, it is of relevance for the understanding of several biological methylation reactions.[94] For intramolecular ion-π interactions two test cases were chosen in which cation-π interactions contribute significantly to the stability of conformations.[58] **18** is based on a study of Dougherty *et al.*,[95] who proposed that the neurotransmitter acetylcholine can bind to acetylcholinesterase through cation-π interactions. A simplified system is taken from Ref. 96, where the folded ester conformation is proposed to be more stable than the unfolded one. For the isosteric 3,3-dimethylbutyl indole-3-acetate (i.e., replaced ammonium nitrogen with carbon), an analogous folding is not observed. This implies that the cationic nature of the quaternary trimethylammonium group is responsible for this preferable association with the indole ring through cation-π interactions. Folded and unfolded conformations were generated with the recently published CREST algorithm.[97] **19** contains multiple interaction motifs that are able to compete with each other. This seesaw balance[98] adopts two distinct conformations that are either stabilized by cation-π or by π-π interactions. Experimental ^{1}H-NMR studies[54,99] in solution proposed that the cation-π bound conformer is stabilized by about 1.5 kcal mol^{-1}.

We are aware that intramolecular ion-π interactions introduce difficulties for fragment based methods such as SAPT. Therefore, full statistics are also given in the ESI† (Table S11, S12) for the IONPI17 set, where the intramolecular test cases (**18** and **19**) are excluded.

Table 1 Summary of the reference interaction and association energies ΔE and methods for the IONPI19 benchmark set. Values are given in kcal mol^{-1}.

System	$\Delta E_{Ref.}$	Estimated error	Reference
1	-39.1	± 0.8 (2.0 %)	37[a)]
2	-25.6	± 0.5 (2.0 %)	37[a)]
3	-19.9	± 0.8 (4.0 %)	37[a)]
4	-14.8	± 0.2 (1.5 %)	90[b)]
5	-25.7	± 0.4 (1.5 %)	90[b)]
6	-19.7	± 0.3 (1.5 %)	90[b)]
7	-21.5	± 0.2 (1.0 %)	this work[c)]
8	-14.6	± 0.2 (1.0 %)	this work[c)]
9	-10.4	± 0.1 (1.0 %)	90[d)]
10	-1.9	< 0.1 (1.0 %)	90[d)]
11	-5.7	± 0.1 (1.0 %)	90[d)]
12	-18.6	± 0.1 (0.5 %)	this work[e)]
13	-33.7	± 0.8 (2.5 %)	this work[f)]
14	-45.0	± 1.1 (2.5 %)	this work[f)]
15	-29.4	± 0.6 (2.0 %)	this work[g)]
16	-26.3	± 0.5 (2.0 %)	this work[g)]
17	-37.2	± 1.9 (5.0 %)	this work[h)]
18	-5.0	± 0.1 (2.5 %)	this work[f)]
19	-2.4	± 0.1 (2.5 %)	this work[f)]
mean	-20.9	± 0.5 (2.2 %)	

a) CCSD(T)/deltaCBS + counterpoise correction (details: see original publication).
b) CCSD(T)/deltaCBS + counterpoise correction + modified frozen core approximation, i.e., Li$^+$ = 1s^2 (no core) and Na$^+$ = [He]2s^{2}2p^6 ([He] core) (details: see original publication).
c) W1-F12.
d) CCSD(T)/deltaCBS + counterpoise correction (details: see original publication).
e) W2-F12.
f) DLPNO-CCSD(T1)/*VeryTightPNO*/CBS(aug-cc-pVTZ/aug-cc-pVQZ).
g) DLPNO-CCSD(T1)/*VeryTightPNO*/CBS(aug-cc-pVTZ/aug-cc-pVQZ) + counterpoise correction and deformation energy.
h) DLPNO-CCSD('T1')/*VeryTightPNO*/'CBS(def2-TZVPP/def2-QZVPP)' + counterpoise correction and deformation energy.

4 Computational details

Typical DFAs from different classes of Jacob's ladder combined with the large def2-QZVPP basis set[100,101] were evaluated for the IONPI19 benchmark set. The DFA selection is based on re-

sults for previous benchmark studies[42] and on their popularity in the computational chemistry community.[102] All DFAs were assessed with the D3 and D4 London dispersion correction in the Becke–Johnson scheme and/or the nonlocal density-dependent NL (VV10) treatment in a non self-consistent form. For M06-L[103] and M06-2X[104] D3 was applied with zero damping.[31] D3 and D4 dispersion corrections were calculated with the `dftd3` and `dftd4` standalone programs.[105] The ORCA[106] implementation was used for ωB97X-D3BJ and to calculate all NL corrections. A list of the tested DFAs and dispersion correction combinations is given in Table 2.

Table 2 Tested DFAs and dispersion correction combinations.

Functional	D3	D4	NL	Reference
composite (3c)				
PBEh-3c	✓	✗	✗	107
B97-3c	✓	✗	✗	59
r^2SCAN-3c	✗	✓	✗	108
(meta-)GGA				
PBE	✓	✓	✓	109
M06-L	✓	✓	✗	103
TPSS	✓	✓	✓	110
r^2SCAN	✓	✓	✓	111,112
B97M	✓	✓	✓	113
hybrid				
M06-2X	✓	✗	✗	104
MN15	✗	✗	✗	114
PBE0	✓	✓	✓	115
PW6B95	✓	✓	✓	116
B3LYP	✓	✓	✓	117,118
ωB97M	✓	✓	✓	119
ωB97X	✓	✓	✓	120
double-hybrid				
B2PLYP	✓	✓	✓	121
revDSD-PBEP86	✗	✓	✗	122
revDSD-BLYP	✗	✓	✗	122
PWPB95	✓	✓	✓	123

All composite ("3c") DFT and r^2SCAN calculations were performed using the TURBOMOLE 7.5.1 program package.[124,125] Computations of energies and geometry optimizations were conducted using the `ridft` and `jobex` programs of TURBOMOLE, respectively. The resolution-of-identity (RI) approximation for the Coulomb integrals was always applied using matching default auxiliary basis sets.[126,127] For the integration of the exchange-correlation contribution, the numerical quadrature grid $m4$ was employed. The default convergence criteria ($10^{-7}\,E_h$ for energies and $10^{-5}\,E_h$/bohr for gradients) were used throughout.

All other DFT, HF, MP2, and local coupled cluster calculations were carried out with the ORCA 4.2.1 program package.[106,128] The frozen core and RI approximations for the correlation part as well as *TightSCF* convergence criteria for the HF energy was employed for all double-hybrids, MP2, and CC methods. The domain based pair natural orbital local coupled cluster method[56] in its sparse maps[57] iterative triples[129] implementation (DLPNO-CCSD(T1)) employing *VeryTightPNO*[60] threshold settings was applied. An aug-cc-pVTZ/aug-cc-pVQZ[130] and def2-TZVPP/def2-QZVPP CBS extrapolation according to the schemes proposed by Helgaker/Klopper[131] (aug-cc basis sets) or Neese/Valeev[132] (def2 basis sets) was carried out for DLPNO-

CCSD(T1). Matching auxiliary basis sets were applied for the density fitting.[133] DLPNO-CCSD(T1)/*VeryTightPNO*/CBS(aug-cc-pVTZ/aug-cc-pVQZ) values were in general counterpoise (CP) corrected unless for the 1:2 (**13**) and 1:3 (**14**) complexes of $C_3F_3N_3$ with Cl$^-$, as the corresponding calculations with and without CP correction for the 1:1 complex (**12**) revealed a negligible residual BSSE of only 0.01 kcal mol^{-1}. Detailed information about the reference calculation for each system are shown in Table 1. To validate the accuracy of the DLPNO-CCSD(T) reference values and to determine if some of the systems show multireference character, a *T1* diagnostic according to Ref. 134 was performed (see ESI† Table S10). Empirically, a value larger than 0.02 may indicate significant nondynamical correlation.[135] This is not the case for the systems in the IONPI19 set, where the largest value is 0.017 for adenine in system **4**. The small to moderate values of the maximum *T2* amplitudes (largest value 0.067 for anthracene in **7**) further indicates that no problematic systems in terms of nondynamical correlation are included in the IONPI19 benchmark.[136]

CBS extrapolation was also performed for MP2. The MP2/CBS schemes correspond to the DLPNO-CCSD(T1) extrapolations for the individual systems. For **1**,**2**, and **6** MP2/CBS(aug-cc-pCVTZ/aug-cc-pCVQZ) was employed without RI since the AutoAux[133] basis showed linear dependencies. For **3** RI-MP2/CBS(aug-cc-pVTZ/aug-cc-pVQZ) was employed for C_6H_6 and RI-MP2/CBS(def2-TZVPPD/def2-QZVPPD) for K$^+$ as no non-relativistic "aug basis" was available. Corresponding auxiliary basis sets were employed. RI-MP2/CBS(aug-cc-pCVTZ/aug-cc-pCVQZ) (AutoAux[133] option in ORCA 4.2.1) was employed for **4** and **5**. For all systems **1**-**6**, the Boys-Bernadi CP correction was applied. The interaction energy of systems **7**-**16** was calculated without CP correction by RI-MP2/CBS(aug-cc-pVTZ/aug-cc-pVQZ) including the corresponding auxiliary basis sets. For **17**, RI-MP2/CBS(def2-TZVPP/def2-QZVPP) was employed including the corresponding auxiliary basis sets, the CP correction, and deformation energy. RI-MP2/CBS(aug-cc-pVTZ/aug-cc-pVQZ) with the corresponding aux basis sets but without CP correction was employed for **18** and **19**. In general, the CP correction was applied only when basis set size or CBS extrapolation were not sufficient enough to minimize the BSSE.

For the largest test system **17**, a slightly more approximate CBS extrapolation scheme was employed for the local coupled cluster correlation energy since the full def2-QZVPP calculation was computationally unfeasible with the latter method. It is labelled as CBS'def2-TZVPP/def2-QZVPP' in the following and refers to a multiplicative scaling of the DLPNO-CCSD('T1') correlation energy by the quotient of the respective CBS(def2-TZVPP/def2-QZVPP) and def2-TZVPP MP2 correlation energies. A similar CBS protocol was already successfully employed in Ref. 58. Note that the iterative correction to the triples correlation energy was calculated with the def2-TZVPP[101] basis set (labeled as 'T1') for this test system. The fact that the iterative triples could only be calculated with the def2-TZVPP basis set introduces a small additional error in the difference between iterative and non-iterative triples, but this is not significant since this correction amounts to 0.5 kcal mol^{-1} only and given that the estimated total error of
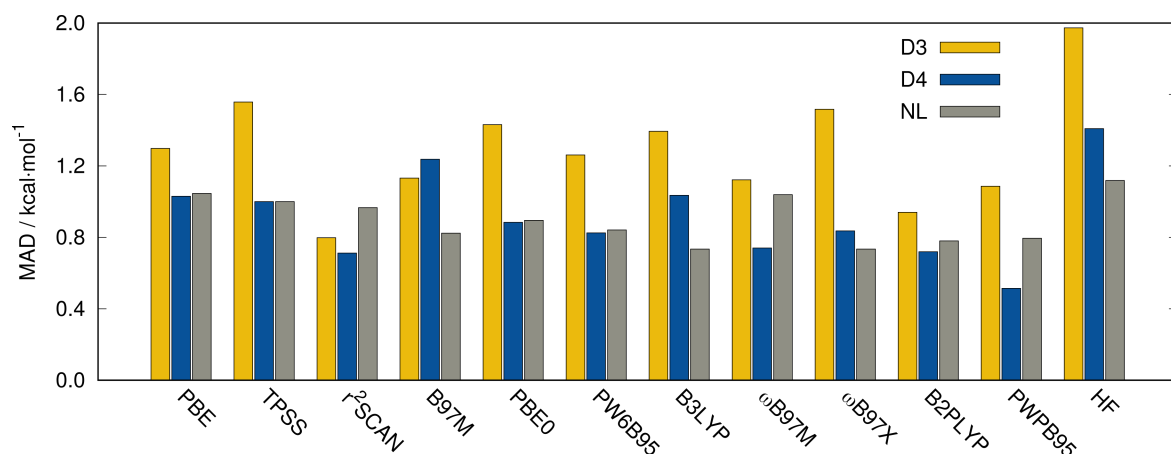
Fig. 3 Comparison of the performance of the D3(BJ), D4(BJ)-ATM, and NL dispersion corrections for different DFAs and HF on the IONPI19 benchmark set.

the total association energy is $\approx$1.9 kcal mol^{-1}. The high-level composite explicitly correlated coupled cluster protocols W1-F12 and W2-F12[55] were applied with the Molpro program package V. 2015.1.[137,138]

For systems **1-6** the Boys-Bernardi counterpoise correction[139] was applied for HF and all non-"3c" DFAs, which do not feature a fixed, composite basis set. This was because the alkali metal ion complexes showed a systematic overestimation of the interaction energy for all assessed DFT methods, which was not observed for the other 13 systems of the IONPI19 set. The CP correction reduced this BSSE on average by 0.3 kcal mol^{-1}. The CP uncorrected values, are given in the ESI† in Table S14. Structures that were newly generated for the IONPI19 benchmark set (**7**, **8**, **12-19**) were all optimized at the PBEh-3c[107] level of theory. Lowest energy molecular conformers were obtained from the advanced conformer rotamer ensemble sampling tool[97,140] (`crest`) in its default settings at the GFN2-xTB[141,142] level followed by DFT geometry re-optimizations at the PBEh-3c level of theory. All SQM and FF calculations were performed with the xtb 6.3.2[143] (GFN1-xTB,[144] GFN2-xTB, GFN-FF[77]), and MOPAC 2016[145] (PM6-D3H4X,[146] PM7[147]) program packages.

5 Results and discussion

In section 5.1 the performance of all tested DFAs and WFT methods for the IONPI19 set is presented and discussed. The dissociation curve of an ion-π complex is shown in section 5.2. SQM and FF methods are evaluated in section 5.3 and a comparison of computation times is given in section 5.4.

5.1 Benchmark study on IONPI19

A representative set of different DFAs including five (meta-)GGAs, seven hybrid functionals, and four double-hybrid (DH) functionals was assessed. In addition, HF and MP2 were tested. Furthermore, the recently developed efficient composite DFT-D methods B97-3c (GGA), r^2SCAN-3c (meta-GGA), and PBEh-3c (hybrid) are evaluated in comparison. Moreover, three correction schemes for capturing long-range London dispersion interactions with DFAs were applied, the D3 correction with Becke-Johnson (BJ) or zero

(0) damping, the newly developed D4 correction with three-body ATM contributions, and the nonlocal dispersion correction (VV10) in its nonself-consistent implementation. First, we want to determine which combination of DFA and dispersion correction works best for the compiled IONPI19 benchmark set. The performance in terms of the mean absolute deviation (MAD) from the reference values of a subset of DFAs, for which all three dispersion corrections are available, is shown in Figure 3.

With a mean MAD of 0.9 kcal mol^{-1} averaged over all 12 tested methods, the recently introduced charge scaled D4 scheme outperforms its predecessor D3, which yields a mean MAD of 1.3 kcal mol^{-1}. Considering the mean interaction energy ΔE of -20.9 kcal mol^{-1}, this improvement is significant. The nonlocal dispersion correction perform on average equally good as the D4 scheme with a mean MAD of also 0.9 kcal mol^{-1}. Yet, this is mostly due to the better performance of the NL correction within the B97M-V and ωB97X-V functionals, which were developed together with the VV10 correction (see Refs. 113, 119). To further investigate the origin of the difference in performance between the D3 and D4 scheme, the role of three-body contributions is taken into account. The results are shown in Figure 4. Here, the ATM term which is default in DFT-D4 was also added to the D3 correction.

Adding the three-body ATM term to the D3 scheme on average improves the mean MAD from 1.3 kcal mol^{-1} to 1.2 kcal mol^{-1}, which is still clearly off the accuracy of the D4-ATM approach with a mean MAD of 0.9 kcal mol^{-1}. As an extension to the ATM term, the many-body dispersion (MBD) approach by Tkatchenko–Scheffler has also been tested[27] in combination with the D4 scheme. Again, the MAD is shown in comparison to respective reference values. Exchanging the ATM term by the MBD approach has nearly no effect, the MADs are only very slightly larger. This proves that the three-body term in D4-ATM is not the reason for the improvement over the D3 scheme for the IONPI19 but the incorporation of atomic partial charges in D4 yielding charge scaled polarizabilities. The rather negligible contribution of three-body effects is further confirmed by the previous discussed good performance of the NL correction, which also does not include
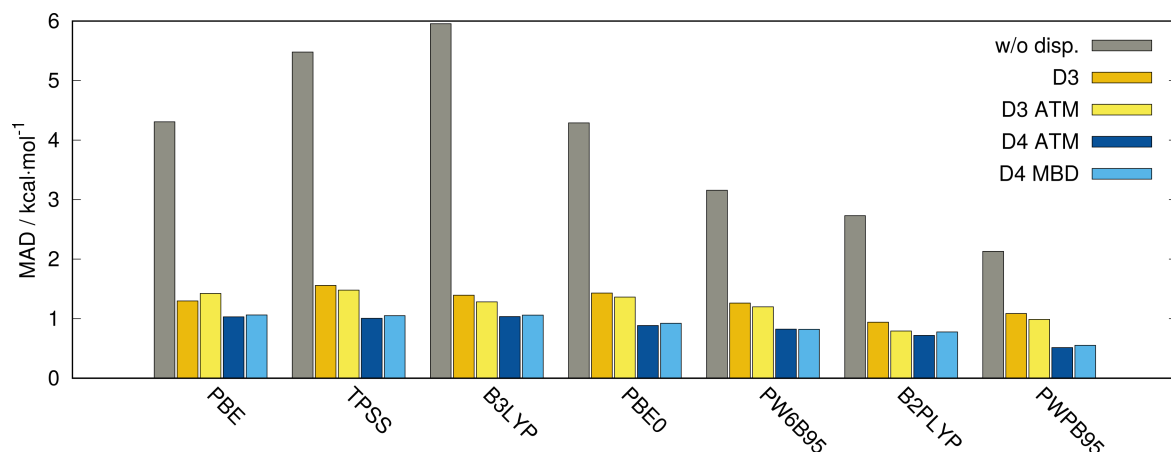
Fig. 4 Comparison of the performance of D3(BJ), D3(BJ)-ATM, D4(BJ)-ATM, and D4(BJ)-MBD dispersion corrections for different DFAs on the IONPI19 benchmark set. The LD-uncorrected results are shown for comparison.

ATM or MBD terms. Another important fact that can be taken from Figure 4 is the general influence of the dispersion correction. It is shown that LD-uncorrected DFT underestimates ion-π interactions significantly, even though electrostatic interactions dominate the overall binding. The mean MAD without an LD correction amounts to 4.0 kcal mol^{-1}. This is in line with SAPT studies, which revealed, that for polarizable systems also LD interactions contribute a crucial part of the ion-π interaction.[39] In general, LD-corrections improve also the Minnesota-type functionals (with D3(0)), although to a smaller extent, since they already capture some dispersion interactions at intermediate interatomic distances by density dependent terms and their parameterization. Yet, on this specific ion-π benchmark no improvement was achieved neither with the D3 nor the D4 scheme. Hence, the LD-uncorrected functionals M06-L, M06-2X, and MN15 will be discussed in the following.

Figure 5 shows the statistical data of the performance for the best combinations of all tested DFA and LD corrections. The efficient composite DFT methods, HF, and MP2 are also included for comparison. The assessed DFAs perform on average as expected according to the picture of "Jacob's Ladder" and resemble closely the results for the extensive GMTKN55 main group benchmark set.[42] The tested (meta-)GGA functionals yield a mean MAD of 1.0 kcal mol^{-1} and mean SD of 1.2 kcal mol^{-1}. With an MAD of 0.7 kcal mol^{-1} the newly developed r^2SCAN-D4 functional is the best performing DFA, closely followed by the B97M-V functional with an MAD of 0.8 kcal mol^{-1}. TPSS-D4 and PBE-D4 perform reasonably well at the limit of chemical accuracy (1.0 kcal mol^{-1}) with 1.0 kcal mol^{-1} and 1.1 kcal mol^{-1}, respectively. The worst among all tested DFAs is M06-L with an MAD of 1.5 kcal mol^{-1}. Also, while most (meta-)GGAs tend to systematically overbind the IONPI19 set (MD < 0), M06-L is the only DFA thereof with a significant positive MD of 1.4 kcal mol^{-1}.

An improvement is obtained with hybrid DFAs. The mean MAD and SD are reduced to 0.8 kcal mol^{-1} and 1.0 kcal mol^{-1}, respectively. The MD is negative for all hybrids, indicating a small systematic error. Out of all tested hybrid DFAs, B3LYP-NL, MN15, ωB97X-V, and ωB97M-D4 perform best with an MAD of

0.7 kcal mol^{-1}, followed by PW6B95-D4 and PBE0-D4 with an MAD of 0.8 and 0.9 kcal mol^{-1}, respectively. The smallest SD is obtained by B3LYP-NL (0.8 kcal mol^{-1}). The global-hybrid MN15 is the best performing Minnesota-type hybrid functional. It clearly improves upon M06-2X (54 % of Fock-exchange), which yields an MAD of 1.1 kcal mol^{-1} and also has the largest MD and SD among all tested hybrid DFAs with -0.9 kcal mol^{-1} and 1.2 kcal mol^{-1}, respectively. Overall, the improvement from (meta-)GGAs to hybrid DFAs is rather small. Hence, the SIE seems to be less severe for the IONPI19 set since the (meta-)GGAs are able to compete with the hybrid functionals. This observation is consistent with the fact that the DFA with the largest amount of Fock-exchange (M06-2X) performs worst. Tentatively it seems that at some point around 30 to 40 % Fock-exchange contribution in the hybrid functional, the results are not improved anymore.

Going to double-hybrid functionals, the mean MAD and SD are further reduced to 0.6 kcal mol^{-1} and 0.8 kcal mol^{-1}, respectively. The best performing DFAs are revDSD-PBEP86-D4 (0.4 kcal mol^{-1} MAD, 0.5 kcal mol^{-1} SD) and PWPB95-D4 (0.5 kcal mol^{-1} MAD, 0.6 kcal mol^{-1} SD), which both nearly approach the accuracy of the reference values. This generally good performance is in agreement with the conclusions of other benchmark studies.[42] revDSD-BLYP-D4 has an MAD of 0.6 kcal mol^{-1} and the DH-DFA with the largest deviation from the reference values is B2PLYP-D4 (0.7 kcal mol^{-1} MAD), whose performance is comparable to the best hybrid DFAs. It is noticeable, that B2PLYP-D4 shows the largest error range out of all DFAs discussed so far. The reason therefore is the overestimation of the association energy of **17** by -5.1 kcal mol^{-1} indicating an outlier of B2PLYP. For **17**, which is the largest system from the test set, a CBS(def2-TZVPP/def2-QZVPP) extrapolation and counterpoise correction were employed for MP2 to correct for the BSSE and basis set incompleteness error. To find out if this is also necessary for double-hybrids which include perturbative correlation energy terms, the same scheme was also applied for PWPB95-D4. The corresponding correction for MP2/CBS amounts to 1.3 kcal mol^{-1}, whereas a correction of only 0.4 kcal mol^{-1} was obtained for PWPB95-D4/CBS, which is less than the mean estimated error of the entire
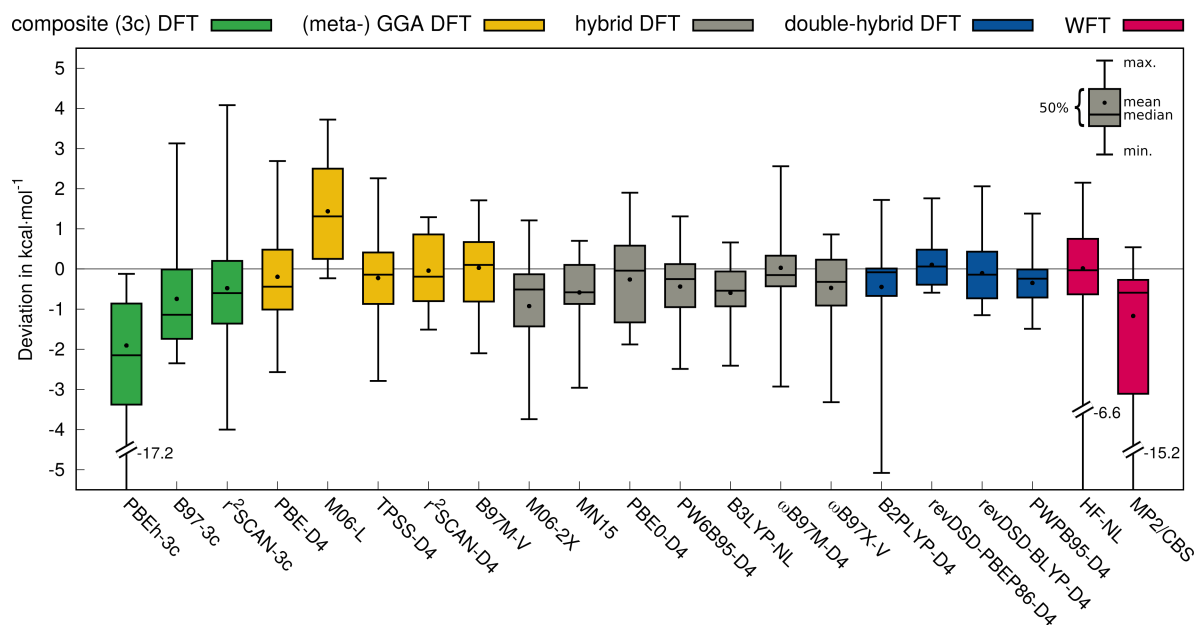
Fig. 5 Deviations of calculated ion-π interaction energies with different DFT and WFT methods for the IONPI19 set. The minimum deviation and maximum deviation for each data set is shown as range together with the first and third quartiles as central box for each data set, the inter-quartile range contains 50 % of the data set. Additionally, the mean and median deviation are depicted as dot and vertical bar, respectively.

IONPI19 set ($\pm$ 0.5 kcal mol^{-1}) Hence for the IONPI19 set, a CBS extrapolation is not necessary for DH-DFAs if they are employed together with the relatively large def2-QZVPP basis set.

The basic philosophy of "3c" composite methods is to provide a consistent description, i.e., without systematic deviations to as low as possible computational cost. Hence, small but well-balanced atomic orbital (AO) basis sets are employed, while the remaining basis set errors are corrected by a geometrical counterpoise correction or in case of B97-3c absorbed into the DFA itself via a slight reparameterization. DFT-3c methods are tested on the IONPI19 set to investigate whether the electrostatics of ion-π interactions are sufficiently described also without large amounts of polarization functions as in the def2-QZVPP basis set. PBEh-3c with its modified SVP basis yields a rather large MAD of 3.5 kcal mol^{-1} and SD of 4.4 kcal mol^{-1}. B97-3c performs already significantly better with a modified TZVP basis, yielding an MAD of 1.4 kcal mol^{-1} (SD = 1.8 kcal mol^{-1}). Best performing "3c" method is the very recently developed r^2SCAN-3c functional with an MAD and SD of 1.3 kcal mol^{-1} and 1.4 kcal mol^{-1}, respectively. Compared to, *e.g.*, the well-established TPSS-D4 meta-GGA with the large def2-QZVPP basis set, r^2SCAN-3c yields only a 0.3 kcal mol^{-1} larger MAD, whilst being one order of magnitude faster. Due to the relatively small but well balanced mTZVP basis, the calculations need only a fraction of computation time compared to the large def2-QZVPP calculations. Hence, the performance of r^2SCAN-3c is promising for large scale computational studies of this type of chemistry. A more detailed look at computation times is given in section 5.4.

For ion-π interactions, the MP2/CBS method (2.0 kcal mol^{-1} MAD) can not reach the accuracy of good DFAs, despite the application of computationally demanding CBS extrapolation schemes. As expected, the ion-π and π-π interactions are systematically

overestimated, a trend which was not observed for DH-DFAs. The largest deviation from the reference is obtained for **17**, where the association energy is overestimated by -15.2 kcal mol^{-1} with MP2/CBS. In general, MP2/CBS can not be recommended for the description of ion-π interactions. Here, DFT good CP corrected DFAs offer higher accuracy at significantly lower computational cost and without CBS extrapolation. Much better results are obtained by HF-NL. The MAD of 1.1 kcal mol^{-1} is comparable to good performing (meta-)GGAs. Since Hartree–Fock is SIE free, the remaining error is mainly due to the comparably poor description of electrostatic interactions.
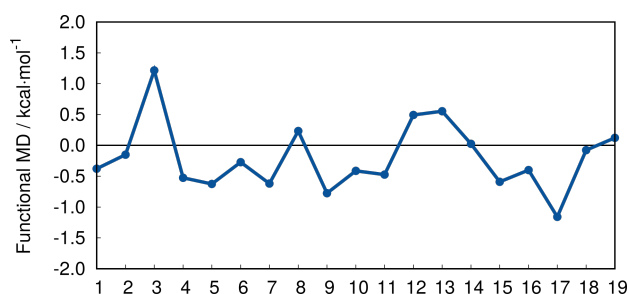

Fig. 6 Functional mean deviation from the reference values calculated as the average of all tested DFAs ("3c" methods excluded).

The calculation of the functional mean deviation (MD) is shown in Figure 6. Here, the deviation from the reference averaged over all DFAs is given per system. The composite DFT methods are excluded due to the different basis set size. The functional mean is a good indication, whether certain subsets (cation, anionic, large systems) or individual systems of the IONPI19 benchmark are particular challenging or show systematic errors. The largely inconspicuous course of the curve presented in Figure 6 indicates a statistically well-balanced test set, without major out-

Table 3 Energy decomposition analyses of the $C_6F_6\cdots Cl^-$ complex for PBE-D4 and PBE0-D4. The total interaction energy (INT), the electrostatic (ES), the Pauli repulsion (REP), the short-range DFA correlation (CORR), and the LD contributions are listed. All values are given in kcal mol^{-1}.

					CMA distance of $C_6F_6\cdots Cl^-$			
	5 a_0		6 a_0		7 a_0		8 a_0	
DFA	PBE	PBE0	PBE	PBE0	PBE	PBE0	PBE	PBE0
INT	-5.1	-5.6	-13.4	-13.5	-11.7	-11.5	-8.7	-8.5
EL	-34.0	-33.5	-12.2	-12.4	-6.1	-6.5	46.3	-4.4
REP	55.8	53.8	13.8	12.9	3.1	2.9	-47.7	0.5
CORR	-24.4	-23.5	-13.1	-12.2	-7.6	-6.7	-6.8	-3.9
LD‡	-3.3	-2.9	-2.5	-2.3	-1.7	-1.6	-1.1	-1.1
Δ^{ref} †	1.9	1.7	0.5	0.6	-0.3	0.0	-0.6	-0.3

† $\Delta^{\mathrm{ref}} = E_{\mathrm{INT}}^{\mathrm{calc}} - E_{\mathrm{INT}}^{\mathrm{ref}}$. ‡ LD contribution calculated with D4.

liers. The average ratio of 1.3 of the MAD to the SD is a further indication of a normal distributed test set.[148] Neither the systems size, nor the anions or cations induce systematic errors. Yet, it is noticeable that the largest functional MDs occur for **3** and **17** with ±1.1, respectively. For many tested DFAs these two systems determine the error range *e.g.*, TPSS-D4, ωB97M-D4, B3LYP-NL, and B2PLYP-D4. System **3** is the only K$^+$ containing complex. Here, the error seems to be attributed more to the def2-QZVPP basis set than to the DFAs.[37] For the largest and most complex system of the IONPI19 set **17**, a proportionally larger error can be expected. The estimated error of the DLPNO-CCSD(T1)/CBS reference amounts to 1.9 kcal mol^{-1} and hence, the functional MD is well below this value.

5.2 Dissociation of ion-π complexes

The results presented for equilibrium geometries (vide supra) did not suggest a major influence of the SIE on the interaction energies of the IONPI19 set. Now, we want to investigate if the SIE becomes more severe for the GGA and meta-GGA classes of DFAs when looking at the dissociation of an ion-π complex. Figure 7 shows the dissociation curves of C_6F_6 and the chloride anion (system **8**) computed with PBE-D4, TPSS-D4, PBE0-D4, and MP2/CBS in comparison to the W1-F12 reference for five different CMA distances within a range of 5 - 8 bohr.

For shorter distances (5 - 6 bohr), all tested DFAs perform similarly and slightly underbind compared to the reference values, whereas MP2/CBS tends to overbind. For larger distances (6 - 8 bohr), all tested methods are reasonably close to the reference. On first sight, also for this system the SIE seems to be less severe since the (meta-)DFAs are able to compete with the hybrid functional (cf. PBE vs. PBE0) and the difference is marginal. To better understand this observation we conducted an EDA[149] for PBE-D4 and PBE0-D4 to investigate the effect of Fock exchange at four CMA distances taken from the dissociation curve in Figure 7 from 5 to 8 bohr, see Table 3).

For all tested CMA distances, PBE0-D4 is only slightly more accurate with an MAD of 0.7 kcal mol^{-1} than PBE-D4 (0.8 kcal mol^{-1}). The EDA interaction energy (INT) is calculated as the sum of electrostatics (EL), Pauli repulsion (REP), DFA correlation (CORR), and LD contributions. Table 3 lists deviations from W1-F12 reference interaction energies (denoted as
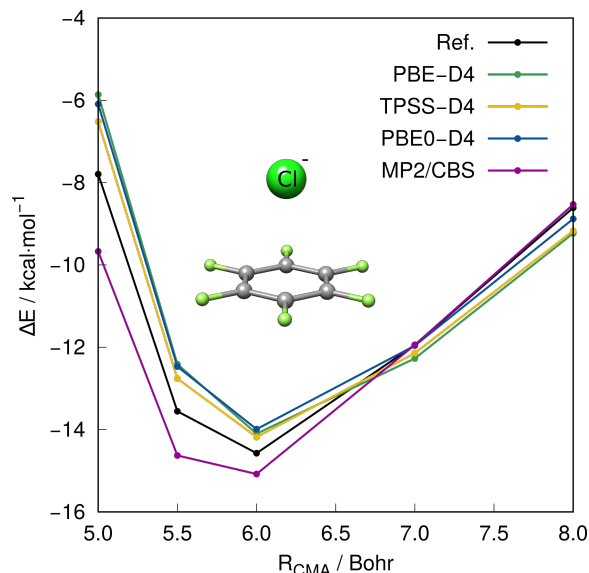

Fig. 7 Intermolecular potential energy curve of C_6F_6 and the chloride anion (Cl$^-$) obtained with PBE-D4, TPSS-D4, PBE0-D4, and MP2/CBS. All DFT calculations were performed in a def2-QZVPP basis set.

$\Delta^{\mathrm{ref}} = E_{\mathrm{INT}}^{\mathrm{calc}} - E_{\mathrm{INT}}^{\mathrm{ref}}$) for both DFAs. At CMA distances of 5, 6, and 7 bohr no significant SIE related issues occur and the energy contributions of PBE-D4 and PBE0-D4 are on the same order of magnitude. This changes, however, for the largest CMA distance of 8 bohr, where PBE-D4 results in nonphysical contributions for EL (repulsive) and REP (attractive) of 46.3 and -47.7 kcal mol^{-1}, respectively. This error is probably due to a violation of the Perdew–Parr–Levy–Balduz condition,[150–154] meaning that the total electronic energy as a function of electron number under a fixed external potential is not interpolating straight between integers. For GGA methods, this usually results in over-delocalization errors[16,155] and thus, the SIE becomes a problem for dissociating ion-π systems. Yet, despite the nonphysical contributions for EL and REP, an accurate PBE-D4 total interaction energy is obtained based on fortuitously error compensation.

5.3 Performance of SQM methods

In recent years, semiempirical QM (SQM) methods have become increasingly popular due to significant improvements in accuracy
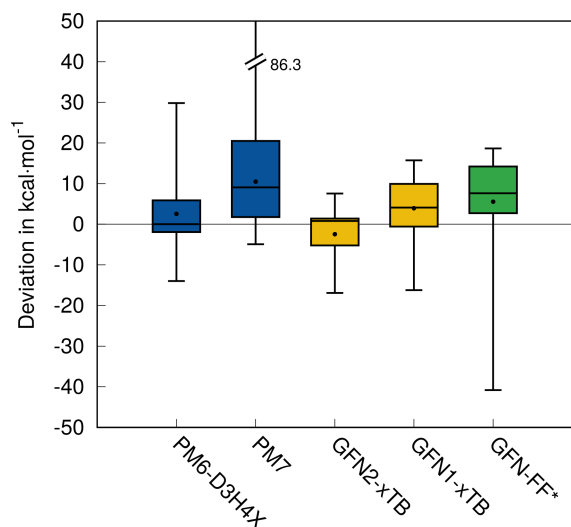
Fig. 8 Deviations of calculated ion-π interaction energies with SQM and FF methods for the IONPI19 set. The minimum deviation and maximum deviation for each data set is shown as range together with the first and third quartiles as central box for each data set, the inter-quartile range contains 50 % of the data set. Additionally, the mean and median deviation are depicted as dot and vertical bar, respectively. The asterisk indicates that systems with wrong topology assignments were excluded for GFN-FF.

Fig. 9 Total wall time for the single point energy of **15** calculated by the best performing methods of each theoretical level in parallel on ten Intel© Xeon E5-2660 v4 @ 2.00 GHz CPUs.

and applicability.[142] Two widely used examples are the NDDO-based PMx [146,147] methods and the more recently developed extended tight-binding methods of the GFNn-xTB [141,142,144] family. The latter proved to be in general more robust and accurate for structure optimization and noncovalent interactions. Recently, also a partially polarizable generic FF has been introduced, termed GFN-FF,[77] which is a promising, generally applicable candidate for a very efficient description of noncovalent interactions. In this section, the performance of the introduced SQM and FF methods is tested for the IONPI19 benchmark set. The statistical data are summarized in Figure 8.

Out of the four tested SQM methods, GFN2-xTB is the best performer with an MAD of 4.7 kcal mol^{-1}, followed by GFN1-xTB (6.8 kcal mol^{-1} MAD). PM6-D3H4X and PM7 show larger deviations from the reference with an MAD of 7.9 and 18.8 kcal mol^{-1}, respectively. With GFN-FF, the topology assignment is initially wrong for the Li$^+$ containing systems **1** and **5**, where the coordination number of Li$^+$ is six rather than zero. Hence, these systems are excluded from the statistical evaluation indicated in Figure 8 by the asterisk. To circumvent wrong topology assignments, the topology file can be generated on the GFN-FF equilibrium structure. For the remaining 17 systems, an MAD of 11.9 kcal mol^{-1} is achieved indicating that for the tested ion-π interactions the classical charge model in GFN-FF reaches is accuracy limits. In comparison to previous studies on mostly neutral NCI complexes,[79] the overall trend among the tested SQM and FF methods is comparable, but the absolute errors are much larger. This is mainly due to the large contribution of the electrostatics to the total interaction energy of ion-π systems. Thus, it is not surprising, that GFN2-xTB performs best out of all tested SQM methods, as it contains a sophisticated multipole electrostatic model. The combina-
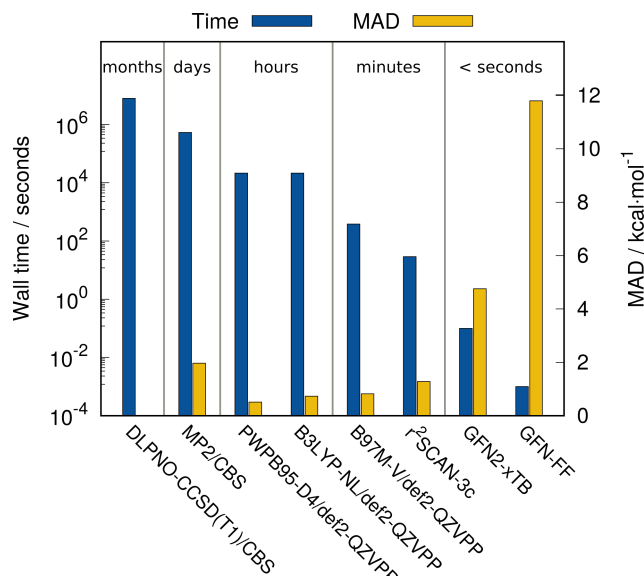
tion of sufficient accuracy with computational efficiency in GFN2-xTB is promising for large scale applications of ion-π interactions in biomacromolecular systems. Nevertheless, the description of electrostatic/induction interactions by SQM and FF methods can not reach the same accuracy as the tested DFAs.

5.4 Timing comparison

The cost to accuracy ratio is evaluated for the best performing methods of the assessed levels of theory. Computational timings for the single point (SP) calculations of **15** are shown in Figure 9 in combination with the respective MAD of the entire IONPI19 set. The wall times are given in seconds on a logarithmic scale and were calculated in parallel on ten CPU cores. With 42 atoms, **15** is well suited as a representative for the IONPI19 set, where the average system size is about 32 atoms per molecule. The calculation of the reference values at the DLPNO-CCSD(T1)/*VeryTightPNO*/CBS(aug-cc-pVTZ/aug-cc-pVQZ) level of theory took about three months. RI-MP2/CBS(aug-cc-pVTZ/aug-cc-pVQZ) calculations lasted more than six days and resulted in an MAD of 1.9 kcal mol^{-1}. DFT methods show significant improvements in the total wall time compared to the MP2/CBS schemes. PWPB95-D4 and B3LYP-NL SP calculations in the large def2-QZVPP basis set converge within a few hours and show lower MADs than MP2/CBS. Here, the double-hybrid PWPB95-D4 is almost as fast as B3LYP-NL, because the MP2 part employing the RI approximation takes up only 5 % of the total wall time. Also the PWPB95-D4 calculation requires one SCF iteration cycle less to converge than B3LYP-NL. The meta-GGA B97M-V SP calculation finishes within ten minutes and the MAD (0.8 kcal mol^{-1}) is still within chemical accuracy (1.0 kcal mol^{-1}). r^2SCAN-3c reaches almost equal accuracy whilst being one order of magnitude faster. With MADs close to chemical accuracy, meta-GGA functionals yield in general the best

cost to accuracy ratio. GFN2-xTB significantly reduces the computational wall time further to less than a second but the underlying approximations increase the MAD to 4.7 kcal mol^{-1}. GFN-FF as the only assessed FF method is yet two orders of magnitude faster than GFN2-xTB.

6 Conclusions

In this work, a comprehensive benchmark set was compiled for a wide range of ion-π interactions. This IONPI19 set represents a diverse set of (bio)chemically relevant molecules, also of larger size and consists of 19 molecular structures that cover inter- as well as intramolecular interactions between anions/cations and π-conjugated systems. The IONPI19 set was used to benchmark various DFAs as well as HF, MP2, SQM, and FF methods. For all DFAs without fixed basis sets and HF, a large def2-QZVPP basis set was applied. In the context of DFT, a main focus was put on the effect of the self-interaction error and of London dispersion interactions for ion-π interactions. Second-order Møller-Plesset perturbation theory extrapolated to the complete basis set limit (MP2/CBS) and Hartree–Fock were evaluated as computationally more expensive but self-interaction error free competitors. Reference interaction and association energies were generated with high-level coupled cluster (CCSD(T)/CBS, W1-F12, W2-F12, and DLPNO-CCSD(T1)/*VeryTightPNO*/CBS) protocols.

First, the effect of different LD corrections was tested and the performance of different DFAs in combination with the D3, D4, and NL dispersion correction schemes were assessed. With a mean MAD of 0.9 kcal mol^{-1} each, the D4 and NL dispersion correction performed equally accurate. In comparison to its predecessor D3, the newly developed D4 model performed consistently better for each tested functional. The difference between these two schemes is mainly due to the inclusion of atomic partial charges in DFT-D4. The incorporation of three- and higher-body dispersion terms was found to have rather small effects. In general the application of a dispersion correction is inevitable for the IONPI19 benchmark, as LD-uncorrected DFT underestimates ion-π interactions significantly and the mean MAD amounts to 4.0 kcal mol^{-1}.

For the IONPI19 set the trend along the Jacob's ladder functional classification scheme was mostly preserved among the tested combinations of DFAs and LD correction meaning that the average performance of (meta-)GGAs (1.0 kcal mol^{-1} MAD) was improved by hybrids (0.8 kcal mol^{-1}MAD), whereas the highest accuracy was reached by the double-hybrids (0.6 kcal mol^{-1} MAD). DH-DFAs reach in many cases an accuracy that is remarkably close to the high-level coupled cluster reference values but at up to two orders of magnitude lower computational cost than MP2/CBS. And, even more importantly, the double-hybrids are also significantly more accurate than MP2/CBS, which systematically and significantly overestimates ion-π interactions (MD = −1.9 kcal mol^{-1}, MAD = 2.0 kcal mol^{-1}). The best cost-to-accuracy ratio was obtained with the newly developed r^2SCAN-3c composite method, which yielded an accuracy close to meta-GGAs like TPSS in a much larger def2-QZVPP basis, whilst being one order of magnitude faster. It was found that the SIE has a relatively small effect on ion-π interactions. This is reflected in the fact that

hybrid DFAs, which include Fock exchange to correct for the SIE, performed only slightly better than (meta-)GGAs. Energy decomposition analysis for the dissociation of ion-π complex **8** further revealed that the SIE of a GGA is rather small for the equilibrium geometry and may become significant only at larger interatomic distances. SQM and FF methods were additionally tested for the IONPI19 set. The simpler description of electrostatic interactions in comparison to DFAs resulted in generally larger errors than obtained in previous studies on neutral systems, as electrostatic interactions are the major contribution of ion-π interactions. The best performing method was GFN2-xTB, which takes into account anisotropic electronic effects by higher order multipole terms.

In conclusion, we generally recommend the use of DH-DFAs with the D4 dispersion correction in a large def2-QZVPP basis set for calculating reference interaction energies of larger (100-250 atoms) ion-π systems. DH-DFAs in combination with D4 extend the possibilities for generating reliable reference values for larger systems, which are essential for the development of low-cost methods to describe ion-π interactions in very large systems such as proteins. This conclusion only really becomes apparent when larger systems are investigated with high-level references as in the presented IONPI19 benchmark set.

Conflicts of interest

There are no conflicts to declare.

Acknowledgements

Notes and references

1 K. Müller-Dethlefs and P. Hobza, *Chem. Rev.*, 2000, **100**, 143–168.
2 M. Rodgers and P. Armentrout, *Chem. Rev.*, 2016, **116**, 5642–5687.
3 O. Gutierrez, J. Aubé and D. J. Tantillo, *J. Org. Chem.*, 2012, **77**, 640–647.
4 C. R. Kennedy, S. Lin and E. N. Jacobsen, *Angew. Chem., Int. Ed.*, 2016, **55**, 12596–12624.
5 R. Goldstein, J. Cheng, B. Stec and M. F. Roberts, *Biochemistry*, 2012, **51**, 2579–2587.
6 C. Estarellas, A. Frontera, D. Quiñonero and P. M. Deyà, *Angew. Chem., Int. Ed.*, 2011, **50**, 415–418.
7 J. A. Faraldos, A. K. Antonczak, V. González, R. Fullerton, E. M. Tippmann and R. K. Allemann, *J. Am. Chem. Soc.*, 2011, **133**, 13906–13909.
8 D. E. Raines, F. Gioia, R. J. Claycomb and R. J. Stevens, *J. Pharmacol. Exp. Ther.*, 2004, **311**, 14–21.
9 S. Tantry, F.-X. Ding, M. Dumont, J. M. Becker and F. Naider, *Biochemistry*, 2010, **49**, 5007–5015.
10 D. Wu, Q. Hu, Z. Yan, W. Chen, C. Yan, X. Huang, J. Zhang,

P. Yang, H. Deng, J. Wang *et al.*, *Nature*, 2012, **484**, 214–219.

11 K. Kapoor, M. R. Duff, A. Upadhyay, J. C. Bucci, A. M. Saxton, R. J. Hinde, E. E. Howell and J. Baudry, *Biochemistry*, 2016, **55**, 6056–6069.

12 C.-C. Chen, W. Hsu, T.-C. Kao and J.-C. Horng, *Biochemistry*, 2011, **50**, 2381–2383.

13 C.-C. Chen, W. Hsu, K.-C. Hwang, J. R. Hwu, C.-C. Lin and J.-C. Horng, *Arch. Biochem. Biophys.*, 2011, **508**, 46–53.

14 N. Mardirossian and M. Head-Gordon, *Mol. Phys.*, 2017, **115**, 2315–2372.

15 S. Grimme and P. R. Schreiner, *Angew. Chem., Int. Ed.*, 2018, **57**, 4170–4176.

16 Y. Zhang and W. Yang, *J. Chem. Phys.*, 1998, **109**, 2604–2608.

17 P. Mori-Sánchez, A. J. Cohen and W. Yang, *J. Chem. Phys.*, 2006, **125**, 201102.

18 J. L. Bao, L. Gagliardi and D. G. Truhlar, *J. Phys. Chem. Lett.*, 2018, **9**, 2353–2358.

19 A. J. Cohen, P. Mori-Sánchez and W. Yang, *Science*, 2008, **321**, 792–794.

20 A. D. Becke, *The Journal of chemical physics*, 2014, **140**, 18A301.

21 S. Grimme, A. Hansen, J. G. Brandenburg and C. Bannwarth, *Chem. Rev.*, 2016, **116**, 5105–5154.

22 E. Rudberg, *J. Phys. Condens. Matter*, 2012, **24**, 072202.

23

24 M. Lundberg and P. E. Siegbahn, *J. Chem. Phys.*, 2005, **122**, 224103.

25 D. R. Lonsdale and L. Goerigk, *Phys. Chem. Chem. Phys.*, 2020.

26 S. Kristyán and P. Pulay, *Chem. Phys. Lett.*, 1994, **229**, 175–180.

27 A. Tkatchenko, R. A. DiStasio Jr, R. Car and M. Scheffler, *Phys. Rev. Lett.*, 2012, **108**, 236402.

28 J. Hermann, R. A. DiStasio Jr and A. Tkatchenko, *Chem. Rev.*, 2017, **117**, 4714–4758.

29 E. R. Johnson, I. D. Mackie and G. A. DiLabio, *J. Phys. Org. Chem.*, 2009, **22**, 1127–1135.

30 S. Grimme, *WIREs Comput. Mol. Sci.*, 2011, **1**, 211–228.

31 S. Grimme, J. Antony, S. Ehrlich and H. Krieg, *J. Chem. Phys.*, 2010, **132**, 154104.

32 S. Grimme, S. Ehrlich and L. Goerigk, *J. Comput. Chem.*, 2011, **32**, 1456–1465.

33 K. Lee, É. D. Murray, L. Kong, B. I. Lundqvist and D. C. Langreth, *Phys. Rev. B*, 2010, **82**, 081101.

34 O. A. Vydrov and T. Van Voorhis, *J. Chem. Phys.*, 2010, **133**, 244103.

35 K. Szalewicz, *WIREs Comput. Mol. Sci.*, 2012, **2**, 254–272.

36 G. Jansen, *WIREs Comput. Mol. Sci.*, 2014, **4**, 127–144.

37 K. U. Lao, R. Schäffer, G. Jansen and J. M. Herbert, *J. Chem. Theory Comput.*, 2015, **11**, 2473–2486.

38 S. E. Wheeler, *Acc. Chem. Res.*, 2013, **46**, 1029–1038.

39 D. Kim, P. Tarakeshwar and K. S. Kim, *J. Phys. Chem. A*, 2004, **108**, 1250–1258.

40 S. Grimme, W. Hujo and B. Kirchner, *Phys. Chem. Chem. Phys.*, 2012, **14**, 4875–4883.

41 E. Perlt, P. Ray, A. Hansen, F. Malberg, S. Grimme and B. Kirchner, *J. Chem. Phys.*, 2018, **148**, 193835.

42 L. Goerigk, A. Hansen, C. Bauer, S. Ehrlich, A. Najibi and S. Grimme, *Phys. Chem. Chem. Phys.*, 2017, **19**, 32184–32215.

43 H. Abbas, *J. Biol. Phys.*, 2017, **43**, 105–111.

44 A. Ferretti, M. d'Ischia and G. Prampolini, *J. Phys. Chem. A*, 2020, **124**, 3445–3459.

45 J. Řezáč, C. Greenwell and G. J. Beran, *J. Chem. Theory Comput.*, 2018, **14**, 4711–4721.

46 S. Tsuzuki, K. Honda, T. Uchimaru and M. Mikami, *J. Chem. Phys.*, 2004, **120**, 647–659.

47 M. O. Sinnokrot and C. D. Sherrill, *J. Phys. Chem. A*, 2004, **108**, 10200–10207.

48 T. Janowski and P. Pulay, *J. Am. Chem. Soc.*, 2012, **134**, 17520–17525.

49 S. M. Cybulski and M. L. Lytle, *J. Chem. Phys.*, 2007, **127**, 141102.

50 A. Heßelmann, *J. Chem. Phys.*, 2008, **128**, 144112.

51 C. Estarellas, X. Lucas, A. Frontera, D. Quiñonero and P. M. Deyà, *Chem. Phys. Lett.*, 2010, **489**, 254–258.

52 M. Goldey and M. Head-Gordon, *J. Phys. Chem. Lett.*, 2012, **3**, 3592–3598.

53 M. Giese, M. Albrecht and K. Rissanen, *Chem. Rev.*, 2015, **115**, 8867–8895.

54 S. Yamada, *Chem. Rev.*, 2018, **118**, 11353–11432.

55 A. Karton and J. M. Martin, *J. Chem. Phys.*, 2012, **136**, 124114.

56 C. Riplinger, B. Sandhoefer, A. Hansen and F. Neese, *J. Chem. Phys.*, 2013, **139**, 134101.

57 C. Riplinger, P. Pinski, U. Becker, E. F. Valeev and F. Neese, *J. Chem. Phys.*, 2016, **144**, 024109.

58 H. Kruse, A. Mladek, K. Gkionis, A. Hansen, S. Grimme and J. Sponer, *J. Chem. Theory Comput.*, 2015, **11**, 4972–4991.

59 J. G. Brandenburg, C. Bannwarth, A. Hansen and S. Grimme, *J. Chem. Phys.*, 2018, **148**, 064104.

60 F. Pavošević, C. Peng, P. Pinski, C. Riplinger, F. Neese and E. F. Valeev, *J. Chem. Phys.*, 2017, **146**, 174108.

61 G. A. Kaminski, R. A. Friesner, J. Tirado-Rives and W. L. Jorgensen, *J. Phys. Chem. B*, 2001, **105**, 6474–6487.

62 H. Minoux and C. Chipot, *J. Am. Chem. Soc.*, 1999, **121**, 10366–10372.

63 R. Sure, J. Antony and S. Grimme, *J. Phys. Chem. B*, 2014, **118**, 3431–3440.

64 K. Kumar, S. M. Woo, T. Siu, W. A. Cortopassi, F. Duarte and R. S. Paton, *Chem. Sci.*, 2018, **9**, 2655–2665.

65 A. Turupcu, J. Tirado-Rives and W. L. Jorgensen, *J. Chem. Theory Comput.*, 2020, **16**, 7184–7194.

66 H. Liu, H. Fu, X. Shao, W. Cai and C. Chipot, *J. Chem. Theory Comput.*, 2020, **16**, 6397–6407.

67 A. D. Becke and E. R. Johnson, *J. Chem. Phys.*, 2007, **127**, 154108.

68 A. D. Becke and E. R. Johnson, *J. Chem. Phys.*, 2007, **127**, 124108.

69 E. Caldeweyher, S. Ehlert, A. Hansen, H. Neugebauer, S. Spicher, C. Bannwarth and S. Grimme, *J. Chem. Phys.*, 2019, **150**, 154122.

70 E. Caldeweyher, C. Bannwarth and S. Grimme, *J. Chem. Phys.*, 2017, **147**, 034112.

71 M. Bursch, E. Caldeweyher, A. Hansen, H. Neugebauer, S. Ehlert and S. Grimme, *Acc. Chem. Res.*, 2018, **52**, 258–266.

72 B. Axilrod and E. Teller, *J. Chem. Phys.*, 1943, **11**, 299–300.

73 Y. Muto, *J. Phys. Math. Soc. Jpn*, 1943, **17**, 629–631.

74 S. Van Gisbergen, J. Snijders and E. Baerends, *J. Chem. Phys.*, 1995, **103**, 9347–9354.

75 S. A. Ghasemi, A. Hofstetter, S. Saha and S. Goedecker, *Physical Review B*, 2015, **92**, 045131.

76 E. Caldeweyher, J.-M. Mewes, S. Ehlert and S. Grimme, *Phys. Chem. Chem. Phys.*, 2020, **22**, 8499–8512.

77 S. Spicher and S. Grimme, *Angew. Chem. Int. Ed.*, 2020, **59**, 15665–15673.

78 S. Spicher and S. Grimme, *J. Phys. Chem. Lett.*, 2020, **11**, 6606–6611.

79 S. Spicher, M. Bursch and S. Grimme, *J. Phys. Chem. C*, 2020, **124**, 27529–27541.

80 S. Spicher, D. Abdullin, S. Grimme and O. Schiemann, *Phys. Chem. Chem. Phys.*, 2020, **22**, 24282–24290.

81 S. Grimme, C. Bannwarth, E. Caldeweyher, J. Pisarek and A. Hansen, *J. Chem. Phys.*, 2017, **147**, 161708.

82 A. D. Becke and E. R. Johnson, *J. Chem. Phys.*, 2005, **123**, 154101.

83 E. R. Johnson and G. A. DiLabio, *Chem. Phys. Lett.*, 2006, **419**, 333–339.

84 E. R. Johnson and A. D. Becke, *J. Chem. Phys.*, 2006, **124**, 174104.

85 A. Otero-de-la Roza and E. R. Johnson, *J. Chem. Phys.*, 2013, **138**, 054103.

86 R. A. DiStasio Jr, V. V. Gobre and A. Tkatchenko, *J. Phys.: Condens. Matter*, 2014, **26**, 213202.

87 K. Berland, V. R. Cooper, K. Lee, E. Schröder, T. Thonhauser, P. Hyldgaard and B. I. Lundqvist, *Rep. Prog. Phys.*, 2015, **78**, 066501.

88 W. Hujo and S. Grimme, *J. Chem. Theory Comput.*, 2013, **9**, 308–315.

89 A. Najibi and L. Goerigk, *J. Chem. Theory Comput.*, 2018, **14**, 5725–5738.

90 B. G. Ernst, K. U. Lao, A. G. Sullivan and R. A. DiStasio Jr, *J. Phys. Chem. A*, 2020, **124**, 4128–4140.

91 B. L. Schottel, H. T. Chifotides and K. R. Dunbar, *Chem. Soc. Rev.*, 2008, **37**, 68–83.

92 D.-X. Wang and M.-X. Wang, *J. Am. Chem. Soc.*, 2013, **135**, 892–897.

93 A. J. Parker, *Chem. Rev.*, 1969, **69**, 1–32.

94 A. McCurdy, L. Jimenez, D. A. Stauffer and D. A. Dougherty, *J. Am. Chem. Soc.*, 1992, **114**, 10314–10321.

95 D. A. Dougherty and D. A. Stauffer, *Science*, 1990, **250**, 1558–1560.

96 K. Aoki, K. Murayama and H. Nishiyama, *J. Chem. Soc., Chem. Commun.*, 1995, 2221–2222.

97 P. Pracht, F. Bohle and S. Grimme, *Phys. Chem. Chem. Phys.*, 2020, **22**, 7169–7192.

98 S. Yamada, N. Yamamoto and E. Takamori, *Org. Lett.*, 2015, **17**, 4862–4865.

99 S. Yamada, N. Yamamoto and E. Takamori, *J. Org. Chem.*, 2016, **81**, 11819–11830.

100 F. Weigend, F. Furche and R. Ahlrichs, *J. Chem. Phys.*, 2003, **119**, 12753–12762.

101 F. Weigend and R. Ahlrichs, *Phys. Chem. Chem. Phys.*, 2005, **7**, 3297–3305.

102 L. Goerigk and N. Mehta, *Aust. J. Chem.*, 2019, **72**, 563–573.

103 Y. Zhao and D. G. Truhlar, *J. Chem. Phys*, 2006, **125**, 194101.

104 Y. Zhao and D. G. Truhlar, *Theor. Chem. Acc.*, 2008, **120**, 215–241.

105 *Generally Applicable Atomic-Charge Dependent London Dispersion Correction* `dftd4`, https://github.com/grimme-lab/dftd4, Accessed: 2021-01-15.

106 F. Neese, *ORCA - An Ab Initio, DFT and Semiempirical electronic structure package, Ver. 4.2.1*, Max-Planck-Institut für Kohlenforschung, Mülheim, Germany, 2020.

107 S. Grimme, J. G. Brandenburg, C. Bannwarth and A. Hansen, *J. Chem. Phys.*, 2015, **143**, 054107.

108 S. Grimme, A. Hansen, S. Ehlert and J.-M. Mewes, *J. Chem. Phys.*, 2021, **154**, 064103.

109 J. P. Perdew, K. Burke and M. Ernzerhof, *Phys. Rev. Lett.*, 1996, **77**, 3865–3868.

110 J. Tao, J. P. Perdew, V. N. Staroverov and G. E. Scuseria, *Phys. Rev. Lett.*, 2003, **91**, 146401.

111 J. W. Furness, A. D. Kaplan, J. Ning, J. P. Perdew and J. Sun, *J. Phys. Chem. Lett.*, 2020, **11**, 8208–8215.

112 S. Ehlert, U. Huniar, J. Ning, J. W. Furness, J. Sun, A. D. Kaplan, J. P. Perdew and J. G. Brandenburg, *J. Chem. Phys.*, 2021, **154**, 061101.

113 N. Mardirossian and M. Head-Gordon, *J. Chem. Phys.*, 2015, **142**, 074111.

114 S. Y. Haoyu, X. He, S. L. Li and D. G. Truhlar, *Chem. Sci.*, 2016, **7**, 5032–5051.

115 C. Adamo and V. Barone, *J. Chem. Phys.*, 1999, **110**, 6158–6170.

116 Y. Zhao and D. G. Truhlar, *J. Phys. Chem. A*, 2005, **109**, 5656–5667.

117 A. D. Becke, *J. Chem. Phys*, 1993, **98**, 5648–5652.

118 C. Lee, W. Yang and R. G. Parr, *Phys. Rev. B*, 1988, **37**, 785.

119 N. Mardirossian and M. Head-Gordon, *J. Chem. Phys.*, 2016, **144**, 214110.

120 N. Mardirossian and M. Head-Gordon, *Phys. Chem. Chem.*

Phys., 2014, **16**, 9904–9924.

121 S. Grimme, *J. Chem. Phys.*, 2006, **124**, 034108.

122 G. Santra, N. Sylvetsky and J. M. Martin, *J. Phys. Chem. A*, 2019, **123**, 5129–5143.

123 L. Goerigk and S. Grimme, *J. Chem. Theory Comput.*, 2011, **7**, 291–309.

124 F. Furche, R. Ahlrichs, C. Hättig, W. Klopper, M. Sierka and F. Weigend, *WIREs Comput. Mol. Sci.*, 2014, **4**, 91–100.

125 *TURBOMOLE V7.5.1 2020, a development of University of Karlsruhe and Forschungszentrum Karlsruhe GmbH, 1989-2007, TURBOMOLE GmbH, since 2007; available from* `http://www.turbomole.com.`, [Online; accessed 06/12/2020].

126 K. Eichkorn, O. Treutler, H. Oehm, M. Häser and R. Ahlrichs, *Chem. Phys.*, 1995, **242**, 652–660.

127 F. Weigend, *Phys. Chem. Chem. Phys.*, 2006, **8**, 1057–1065.

128 F. Neese, *WIREs Comput. Mol. Sci.*, 2018, **8**, e1327.

129 Y. Guo, C. Riplinger, U. Becker, D. G. Liakos, Y. Minenkov, L. Cavallo and F. Neese, *J. Chem. Phys.*, 2018, **148**, 011101.

130 R. A. Kendall, T. H. Dunning and R. J. Harrison, *J. Chem. Phys.*, 1992, **96**, 6796–6806.

131 T. Helgaker, W. Klopper, H. Koch and J. Noga, *J. Chem. Phys.*, 1997, **106**, 9639–9646.

132 F. Neese and E. F. Valeev, *J. Chem. Theory Comput.*, 2011, **7**, 33–43.

133 G. L. Stoychev, A. A. Auer and F. Neese, *J. Chem. Theory Comput.*, 2017, **13**, 554–562.

134 T. J. Lee and P. R. Taylor, *Int. J. Quantum Chem.*, 1989, **36**, 199–207.

135 P. Gersdorf, W. John, J. P. Perdew and P. Ziesche, *Int. J. Quantum Chem.*, 1997, **61**, 935–941.

136 U. R. Fogueri, S. Kozuch, A. Karton and J. M. Martin, *Theor. Chem. Acc.*, 2013, **132**, 1–9.

137 H. J. Werner, P. J. Knowles, G. Knizia, F. R. Manby and M. Schütz, *WIREs Comput. Mol. Sci.*, 2012, **2**, 242–253.

138 *Molpro V15.1 2015, a package of ab initio programs; available from* `http://www.www.molpro.net.`, [Online; accessed 05/06/2020].

139 S. F. Boys and F. Bernardi, *Mol. Phys.*, 1970, **19**, 553–566.

140 *Conformer-Rotamer Ensemble Sampling Tool based on the xtb Semiempirical Extended Tight-Binding Program Package* `crest`, `https://github.com/grimme-lab/crest`, Accessed: 2021-01-15.

141 C. Bannwarth, S. Ehlert and S. Grimme, *J. Chem. Theory Comput.*, 2019, **15**, 1652–1671.

142 C. Bannwarth, E. Caldeweyher, S. Ehlert, A. Hansen, P. Pracht, J. Seibert, S. Spicher and S. Grimme, *WIREs Comput. Mol. Sci.*, 2021, **11**, e1493.

143 *Semiempirical Extended Tight-Binding Program Package* `xtb`, `https://github.com/grimme-lab/xtb`, Accessed: 2021-01-15. See also xTB Documentation available at https://xtb-docs.readthedocs.io/en/latest/.

144 S. Grimme, C. Bannwarth, E. Caldeweyher, J. Pisarek and A. Hansen, *J. Chem. Phys.*, 2017, **147**, 161708.

145 J. J. P. Stewart, *MOPAC2016*, Stewart Computational Chemistry, Colorado Springs, CO, USA, 2016.

146 J. Řezáč and P. Hobza, *J. Chem. Theory Comput.*, 2012, **8**, 141–151.

147 J. J. P. Stewart, *J. Mol. Model.*, 2013, **19**, 1–32.

148 R. C. Geary, *Biometrika*, 1935, **27**, 310–332.

149 P. Su and H. Li, *J. Chem. Phys.*, 2009, **131**, 014102.

150 J. P. Perdew, R. G. Parr, M. Levy and J. L. Balduz Jr, *Phys. Rev. Lett.*, 1982, **49**, 1691.

151 Y. Zhang and W. Yang, *Theor. Chem. Acc.*, Springer, 2000, pp. 346–348.

152 W. Yang, Y. Zhang and P. W. Ayers, *Phys. Rev. Lett.*, 2000, **84**, 5172.

153 J. P. Perdew, A. Ruzsinszky, G. I. Csonka, O. A. Vydrov, G. E. Scuseria, V. N. Staroverov and J. Tao, *Phys. Rev. A*, 2007, **76**, 040501.

154 A. J. Cohen, P. Mori-Sánchez and W. Yang, *Phys. Rev. B*, 2008, **77**, 115123.

155 E. R. Johnson, P. Mori-Sánchez, A. J. Cohen and W. Yang, *J. Chem. Phys.*, 2008, **129**, 204112.